A simulation model for thickness profile of the film deposited using planar circular type magnetron sputtering sources

Seungbum Hong,[a)] Eunah Kim, Byeong-Soo Bae, and Kwangsoo No
Department of Material Science and Engineering, KAIST, Kuseong-dong, Yusong-gu, Taejon, South Korea

Sung-Chul Lim, Sang-Gyun Woo, and Young-Bum Koh
Samsung Electronics Co., Ltd., Yongin-gun, Kyongki-do, South Korea

(Received 31 October 1995; accepted 21 June 1996)

The thickness profile of the film deposited by planar circular-type magnetron is simulated considering the relationship between magnetic field profile and target erosion rate. The model is confirmed by the measurement of the film thickness profiles of the Cr films deposited in this study. It is found that the model is applicable to the magnetron sputtering process at low gas pressure. Furthermore, it can be used to predict the thickness profile of the films deposited by magnetron sputtering with various shapes of magnets. © *1996 American Vacuum Society.*

I. INTRODUCTION

Recently, magnetron sputtering has been widely used in thin film fabrication since it offers high deposition rate and operates at lower pressure than the conventional one without magnetron. The manifestation of the relationship between the main film quality (mechanical, electrical, optical properties, etc.) and the deposition parameters (total chamber pressure, gas flow rate, target-substrate distance, etc.) is required to control the process more efficiently. Especially, among the main film quality, the thickness uniformity of the film is a critical factor in optical applications because it is directly relevant to the optical properties of the film such as transmittance, absorption, and refractive index, etc.

Much theoretical and experimental research has been performed to investigate the film thickness distribution.[1–4] Heberlein *et al.*[1] used the Monte-Carlo method to simulate the film thickness, as well as angular and energy distributions. They divided the magnetron sputtering process into three parts; particle emission from target, gas scattering, and film growth. Furthermore, they took the cosine distribution function for emission characteristics, Thompson's relation for emission probability, erosion depth profile for erosion rate, elastic gas scattering between sputtered particles and background gas particles, and particle losses by chamber wall deposition or thermalization. Fursenko *et al.*[2] also used the Monte-Carlo method, but they added some hydrodynamic concept into their simulation. They took the emission characteristics to be a cosine-emitting distribution function and assumed the background gas to be a continuum media with hyposonic flow, focusing on the transport of gases at low pressure and at medium pressure. In the low-pressure region, the linear Boltzmann equation and the Poisson distribution were used to describe the transport process of the particles and the collision between the Monte Carlo test particles and background gases. In the medium pressure region, the test particle Monte Carlo method was utilized for the kinetic regime and convective diffusion equation for the diffusion regime that occurs after thermalization. Fan *et al.*[3] and Swann *et al.*[4] assumed no gas scattering, cosine emitting source, and calculated the erosion rate from the erosion depth profile.

Most of the authors have calculated the target erosion rate from the target erosion depth profile. Though it has been mentioned by many authors that the target erosion rate is dependent on the magnetic field profile, there is almost no quantitative work on their relationship. Therefore, in this study the role of the magnetic field profile and its relationship with the erosion rate has been considered in simulating the thickness profile of the film deposited by the planar circular-type magnetron sputtering system. Then, the validity of the model was confirmed by the measurement of the Cr film thickness profiles after sputter deposition.

II. MODEL DEVELOPMENT

In this study, several assumptions have been taken to simplify the model. These are (1) no gas phase collisions, (2) unit sticking coefficient, (3) cosine-emitting source,[5] and (4) linear proportionality between loop current density and etch rate.

A. Cosine-emitting source and plane parallel receiver (Ref. 6)

Let F_0 denote the flux of the sputtered atoms from the source per steradian in the direction perpendicular to the source plane. It is assumed that Knudsen's cosine law of evaporation is valid for each elemental area, ΔA_S, of a planar emitting surface and that the source is planar, circular, and uniform. Then the flux of sputtered atoms from the area of the source element, ΔA_S, to the area of the receiver element, ΔA_R, should be

$$d\Delta H = \frac{F_0 \Delta A_R d^2}{(r^2 - 2rx\cos\phi + x^2 + d^2)^2} \times r\,d\phi\,dr \quad \text{(mol/s)}, \tag{1}$$

where ΔH is the total flux from the source to the area of the receiver element ΔA_R, r is the radial distance of the source element from the origin on its plane, x is the projected length to the x axis of the line connecting the origin on the source

a)Electronic mail: seungbum@cais.kaist.ac.kr

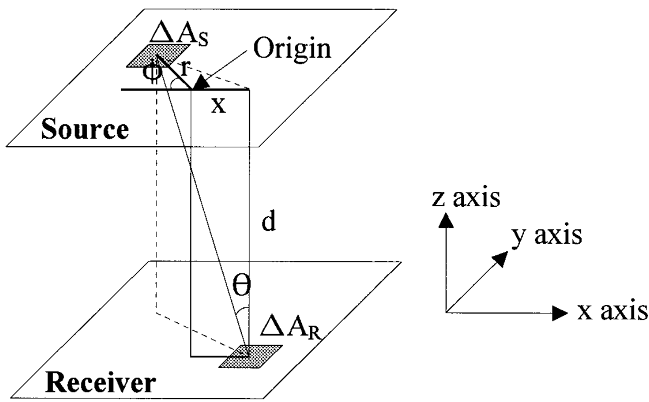

FIG. 1. Plane source with parallel, plane receiver (see Ref. 6).

plane and the central point of the receiver element, d is the source to receiver distance, and ϕ is the angular coordinate of the source element[6] (Fig. 1).

B. Nonuniform source and plane parallel receiver

In Eq. (1), it was assumed that a uniform source is present, but modification of Eq. (1) is necessary for the nonuniform magnetron sputtering system. The coexistence of the magnetic field and the local electric field causes electrons to hop around the source plane, which induces the local current of electrons, as shown in Fig. 2. This is the reason that a high plasma density region is formed in a loop shape on the source plane. The plasma density in this region called etch track is so high that the etch rate caused by only the electric field can be ignored in comparison to that done by the combination of the electric field and the magnetic field.

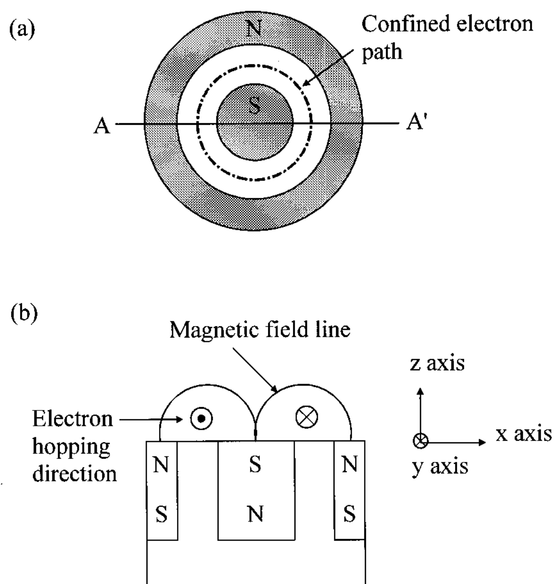

FIG. 2. Schematic diagram of (a) planar circular magnetron and (b) its cross-sectional view along A-A'.

The loop current density, as defined in Eq. (2), is linear in ion/electron density, which in turn shows a linear relationship with the local sputter rate, thus the loop current density is proportional to the etch rate. Current density along the y axis in the configuration shown in Fig. 2 can be expressed as the following:

$$J_y = n_e e v_y, \tag{2}$$

where n_e is electron concentration, e is the electron charge, and v_y is the electron velocity along the y axis. In this case, the source plane is taken to be the xy plane, and the surface normal of the source plane to be the z direction. The hopping direction of the electrons is assumed to be parallel to the y axis. We also assume that the electric field in the dark space decreases linearly across the dark space thickness, L.[7] Letting the target surface be $z=0$ gives

$$E_z = -E_0\left(1-\frac{z}{L}\right), \tag{3}$$

where E_0 is the absolute value of the field at the target. Moreover, if we assume that the electron emission velocity at the surface of the source plane is zero, the equation of motion becomes

$$\frac{d^2y}{dt^2} = -\frac{eB_x \frac{dz}{dt}}{m_e}, \tag{4}$$

which yields

$$\frac{dy}{dt} = v_y = -\frac{eB_x z}{m_e}. \tag{5}$$

Considered the electron motion along the z axis

$$m_e \frac{d^2z}{dt^2} = -eE_z + eB_x \frac{dy}{dt}. \tag{6}$$

Solving the differentiated equation in combination with Eqs. (3), (4), (5), and (6), we may solve the velocity

$$v_y = -\frac{e^2E_0B_x}{m_e^2\omega^2}(1-\cos\omega t), \tag{7}$$

where

$$\omega^2 = \frac{eE_0}{m_eL} + \frac{e^2B_x^2}{m_e^2}. \tag{8}$$

In this study, the maximum B field at the surface of the source plane was 176.5 G. The dark space thickness at the condition of discharge voltage of 500 V and total chamber pressure of 1.3 Pa was 0.376 mm.[8] Using the Langmuir probe, the plasma potential was measured to be 10 V. Therefore, under this condition, the ratio of the second term to the first term in Eq. (8) is given by

$$\text{ratio}=\frac{\frac{e^2B_x^2}{m_e^2}}{\frac{eE_0}{m_eL}}=\frac{LeB^2}{m_eE_0}=\frac{L^2eB^2}{m_e(V+V_p)}$$

$$=\frac{(0.376\times10^{-3})^2\times1.6\times10^{-19}\times(1.765\times10^{-2})^2}{9.11\times10^{-31}\times(500+10)}$$

$$=0.0152.$$

Since the value of the second term is found to be about 1.5% of that of the first term, the second term can be ignored in Eq. (8). This makes ω to be constant independent of the B field. Therefore, the time-averaged mean velocity becomes

$$\overline{v_y}=-\frac{e^2E_0B_x}{m_e^2\omega^2}=\alpha B_x, \tag{9}$$

where a proportional constant, $\alpha=-e_2E_0/m_e^2\omega^2$. Thus, the mean current density becomes

$$\overline{J_y}=n_ee\overline{v_y}=n_ee\alpha B_x=\beta B_x, \tag{10}$$

where a proportional constant, $\beta=n_ee\alpha$.
According to the assumption that the etching rate of the source plane is proportional to the loop current density, it is found that the etching rate of the source plane increases linearly with the magnetic field component being parallel to the source plane. In the case of the planar and circular magnetron sputtering system, it can be inferred that

$$\overline{J_\theta}=\beta B_r \tag{11}$$

and the modified form of Eq. (1) is given by

$$d\Delta H=\chi\frac{B_r\Delta A_Rd^2}{(r^2-2rx\cos\phi+x^2+d^2)^2}\times rd\phi dr, \tag{12}$$

where χ is a proportional constant.

C. Magnetic field measurement and polynomial approximation of the magnetic field

In this study, magnetic field was measured using a Gaussmeter (Fig. 3). We have adopted the polynomial approximation method to fit the radial component of the magnetic field at the surface of the source. Thus, the approximated quadratic function for the region of interest is

$$B_r=-1.30\times10^{-4}\times(r^2-22.5r)\quad\text{(Tesla)}, \tag{13}$$

as shown in Fig. 3.

D. Indefinite integral and finite elemental method

The circular symmetry of the source makes the evaluation along one projected source radius describing completely the distribution over the receiver surface. Thus, Eq. (12) is suitable for our purpose. The integration of Eq. (12) over ϕ from 0 to 2π, exclusive of the coefficient $\chi\Delta A_Rd^2$, gives[9]

$$\frac{\Delta H}{\chi\Delta A_Rd^2}=2\pi\int\frac{B_r(r^2+x^2+d^2)rdr}{[r^4-2r^2(x^2-d^2)+(x^2+d^2)^2]^{3/2}}. \tag{14}$$

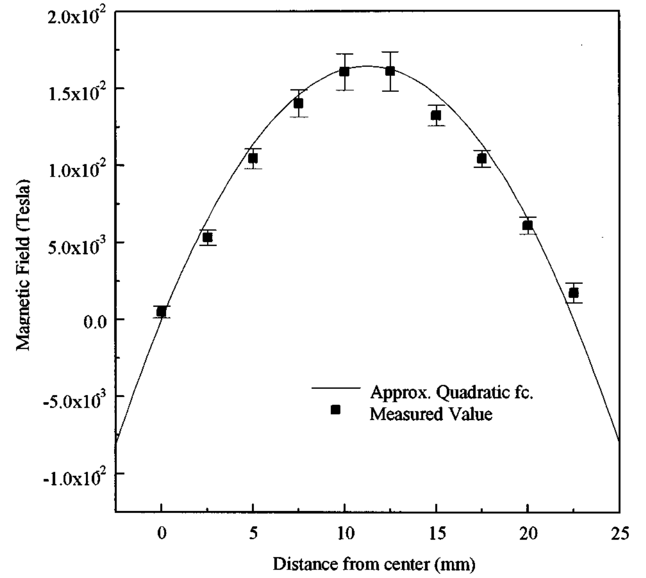

FIG. 3. Distribution profile of x axis component of the magnetic field.

A combination of Eqs. (13) and (14) will yield the following equation:

$$\frac{\Delta H}{\chi\Delta A_Rd^2}=-2\pi\times\int_0^{22.5}\frac{1.30\times10^{-4}(r^2-22.5r)(r^2+x^2+d^2)rdr}{[r^4-2r^2(x^2-d^2)+(x^2+d^2)^2]^{3/2}}. \tag{15}$$

This can be divided into two parts

$$\frac{\Delta H}{\chi\Delta A_Rd^2}=-2\pi\int_0^{22.5}\frac{1.30\times10^{-4}r^2(r^2+x^2+d^2)rdr}{[r^4-2r^2(x^2-d^2)+(x^2+d^2)^2]^{3/2}}+2\pi\int_0^{22.5}\frac{1.30\times10^{-4}\times22.5r(r^2+x^2+d^2)rdr}{[r^4-2r^2(x^2-d^2)+(x^2+d^2)^2]^{3/2}}. \tag{16}$$

Letting $\xi=r^2$, the first term can be integrated in two parts[9] to give

$$-1.30\times10^{-4}\left\{\pi\frac{\xi(\xi-C)}{(C-D)R^{1/2}}-\frac{1}{(C-D)}\times[\sqrt{R}+(D-C)\ln(2\sqrt{R}+2\xi-2D)]\right\}_0^{22.5^2}, \tag{17}$$

where C is x^2+d^2, D is x^2-d^2, and R is $\xi-2\xi D+C^2$. The second term in Eq. (16) is found to be not solved by an analytical method. Therefore, we used a finite element method to evaluate the second term.

III. EXPERIMENT

Cr films were prepared using a planar circular type magnetron sputtering system with a ring-shaped 2 in. target. The outside diameter of the Cr target was 50.8 mm and the inside

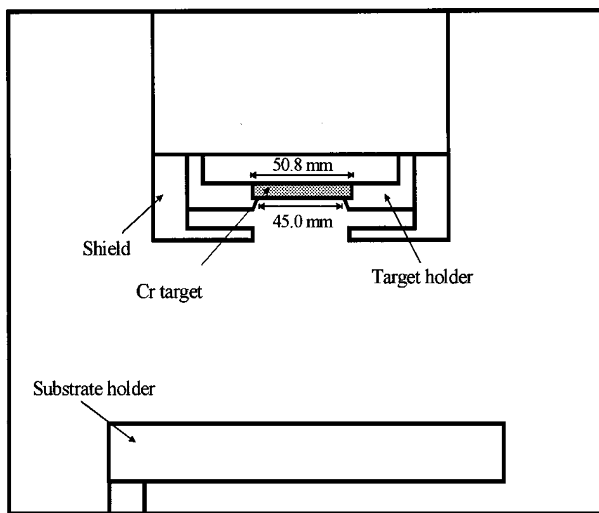

FIG. 4. Schematic diagram of the sputtering system.

diameter was 45.0 mm with the thickness of 6.2 mm (Fig. 4). The films were deposited at the condition of discharge voltage of 500 V, discharge current of 0.1 A, and total chamber pressure of 1.3 Pa. The reason the total chamber pressure was chosen to be 1.3 Pa is that the lowest total chamber pressure is required to minimize the collision effect of the gas phase and it was found to be 1.3 Pa in our system. The target to substrate distance was varied with 50, 80, and 100 mm. The deposition was conducted at the ambient temperature. The thickness profiles of the films were measured by Tencor alpha-step instrument. Four data points were taken and averaged for each sampling point to provide credibility of the measured data. Moreover, all the films were deposited in sufficient time to yield the thickness of over 5000 Å because the variation of thickness was usually under 50 Å. The measured thickness profile was normalized with the highest thickness value to be compared with the simulated profile.

IV. RESULTS AND DISCUSSIONS

Uniformity of the film thickness over an area as large as possible is a basic demand in thin film technology. One of the major factors which influence the uniformity is the variation of the target-substrate distance.[6] The assumptions such as no gas phase collisions, unit sticking coefficient, cosine-emitting source, and linear proportionality between loop current density and target erosion rate were taken into account. While deriving the film thickness distribution equation, we correlated the magnetic field and the erosion rate quantitatively. This enabled us to predict the film thickness profile of magnetron sputtering equipped with various shapes of magnets.

A. Model verification and applicability

The verification of the model can be done by comparing the experimental data and theoretical values of thickness profile at some different conditions. Since no gas phase scattering is assumed in the model, the Knudsen number[2,10] of each

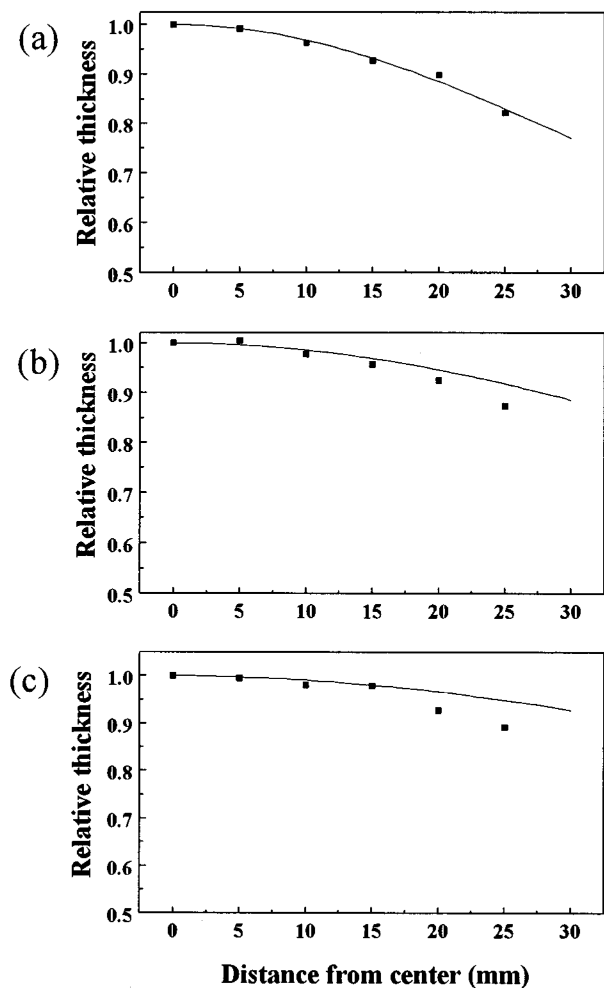

FIG. 5. Simulated and measured thickness profile for different target to substrate distance of (a) 50 mm, (b) 80 mm, and (c) 100 mm.

condition should be large to ensure the assumption. To evaluate the Knudsen number of each condition the mean free path for sputtered Cr atoms must be calculated. From the well known equation for the mean free path,[11] one can calculate it if the collision cross section and the background gas density are given. Consequently, taking the gas phase collision as being elastic, we will calculate the elastic cross section and the background gas density to evaluate the mean free path of sputtered Cr atoms. Moreover, we will present the pressure ranges in terms of Knudsen number so that the model can be applied more reliably.

1. Calculation of the elastic cross section

Assuming Thompson distribution[12] of the sputtered Cr atoms, the average sputtered energy is calculated to be 11.93 eV with the surface binding energy of 4.2 eV.[12] This value of average sputtered energy for Cr is very close to 11 eV measured by Thornton *et al.*[13] Since the elastic cross section varies with the log scale of the sputtered energy,[14] a relatively rough estimation would be sufficient to calculate the cross section. With a similar approach performed by Rossnagel,[15]

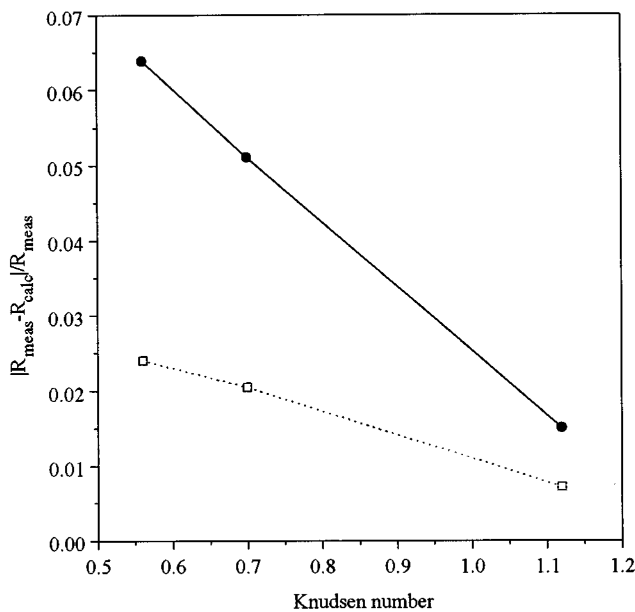

FIG. 6. The absolute deviation of the predicted values from the measured data vs. Knudsen number. R, the relative flux, ●, the maximum absolute deviation among sampling points, □, the average absolute deviation over the sampling points.

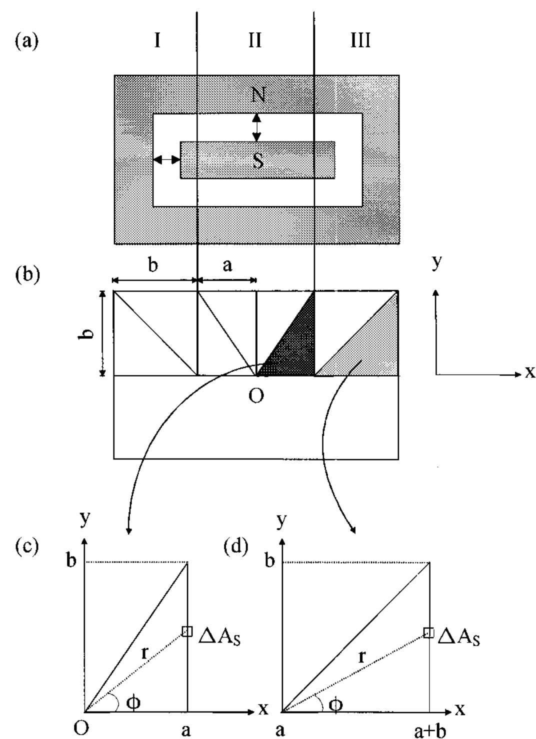

FIG. 7. Schematic diagram of (a) rectangular magnetron sputtering configuration and (b) its overview with magnified pictures of triangular regions of (c) segment II and (d) segment III.

the cross section for Cr atoms of 11.93 eV is found to be 6.0×10^{-16} cm^2 from the work of Robinson.[14]

2. Calculation of the background gas density

Before calculating the background gas density, the gas rarefaction effect should be taken into account. While the magnetron discharge current of 0.1 A is not expected to contribute to a significant change in the background gas density, it is found to reduce the background gas density to 83% of the original value at 1.3 Pa for Cu sputtering in Ar.[15] Considering the average sputtered energy, momentum transfer cross section,[14] and sputtering yield of Cr,[16] we can evaluate the reduction factor of the background gas density to be 0.90 from the work of Rossnagel,[15] which is a bit higher value than that of Cu at the condition of interest. It is equivalent to say that the background gas density is reduced to 3×10^{14}/cm^3 from 3.3×10^{14}/cm^3 at 1.3 Pa.

3. Verification and applicability of the model

It is found that the mean free path for 11.93 eV Cr atoms in Ar at 1.3 Pa with 0.1 A of magnetron discharge current is about 5.6 cm from the above calculations. This value is comparable to 4.5 cm at 1.3 Pa (inferred from the 1.5 cm at 4 Pa) for Cu atoms calculated by Rossnagel[15] without considering the gas rarefaction effect (it will increase up to 5.4 cm if the gas rarefaction is taken into account). Eventually, the Knudsen number will vary from 0.56 to 1.12 with target-substrate distance variation from 10 to 5 cm at the above given deposition condition.

A large Knudsen number over 1 which ensures molecular flow of the background gas would be the primary condition for verification and application of our model. However, it was very difficult either to lower the pressure below 1.3 Pa or to reduce the substrate-target distance below 5 cm in our system so that there was no method to perform experiments where the Knudsen number reaches far beyond 1. Recently, there have been developed many magnetron sputtering devices which operate at very low pressure (less than 0.1 Pa)[17] and this model may be more suitable for such equipment. Nonetheless, though not perfectly matched, the simulated profile was matched to the experimental results quite well, as shown in Fig. 5. It is found that as the target to substrate distance increases, the discrepancy between the experimental and the simulated values increases. This trend is shown in Fig. 6 in terms of the deviation versus the Knudsen number. The deviations between the predicted values and the experimental data showed a linear dependence with the Knudsen number. Moreover, the points far from the center are found to have more deviated values from the simulated ones. These may be attributed to the fact that the model is less valid as the collision frequency increases. If we take 3% as a tolerable limit for maximum deviation in the film thickness profile, it is found that the Knudsen number should be at least 1 for application of this model as is expected from the above discussion.

B. Application for other magnetron geometry

As mentioned above, this model may be applied not only to circular magnetron systems but also to noncircular mag-

netron systems such as rectangular ones. Rectangular magnetron can be thought of as a combination of linear magnetrons of parallel-type and perpendicular-type with respect to the sampling direction of the thickness profile (Fig. 7). The deposition profile can be obtained by summing the fluxes contributed by each segment divided, as shown in Fig. 7. Segments I and III represent the areas where the magnetic field is a function of both x and y coordinates of the point of interest, while segment II represents the area where it is an only function of its y coordinate. The dimension of each segment can be given, as shown in Fig. 7(a), because the width of the open space [denoted by arrows in Fig. 7(a)] between magnetrons is usually the same.

Since the magnetrons beneath the target have a mirror symmetry with respect to the x axis, the total flux from the target can be calculated by doubling the flux from the upper half part of the target [Fig. 7(b)]. The flux from each segment will be treated in detail, and the equation for the total flux will be given in the form of an integral which necessitates the use of the finite elemental method.

1. The sputtered flux from segments I and III in Fig. 7

It is necessary to divide the area of integration into two triangular regions to use the circular coordinate (r,ϕ) for integration in the case of segments I and III. However, only the light gray triangle in Fig. 7(b) will be discussed in detail, and then the total flux from segments I and III will be given without further details. First of all, the upper limit for r in the integration of Eq. (12) is a function of ϕ and is equal to $b/\cos\phi$, hence the limits of the integration over r is 0 to $b/\cos\phi$. Also, it can be easily shown that the limits for ϕ in the integration is 0 to $\pi/4$ from Fig. 7(d). Secondly, the x axis is shifted by a value of "a," thus the "x" in Eq. (12) should be replaced by "$x-a$." However, the x axis shift is in the reverse direction for segment I and, accordingly, the "x" should be replaced by "$x+a$." Thirdly, assuming that the maximum value of the B field, $B_{\max}$, in the r axis is constant with a small variation of the distance between the "N" pole and "S" pole of the magnetrons, the equation for the B_r will be

$$B_r=-(\text{const})r\left(r-\frac{b}{\cos\phi}\right). \tag{18}$$

Therefore, the flux from the light gray triangular component in Fig. 7 will be

$$\Delta H=\int_0^{\pi/4}\int_0^{b/\cos\phi}\chi\frac{r\left(r-\frac{b}{\cos\phi}\right)d^2}{[r^2-2r(x-a)\cos\phi+(x-a)^2+d^2]^2}\,rdrd\phi. \tag{19}$$

If we denote the denominator of the integrand in Eq. (12) as $f(r,x,d,\phi)$ then the total flux from segments I and III will be

$$\begin{aligned}\Delta H=\Delta H_{\mathrm{I}}+\Delta H_{\mathrm{III}}=2\chi\Bigg[&\int_0^{\pi/4}\int_0^{b/\cos\phi}\left\{\frac{r\left(r-\frac{b}{\cos\phi}\right)d^2}{f(r,x+a,d,\phi)}\right\}rdrd\phi+\int_{\pi/4}^{\pi/2}\int_0^{b/\sin\phi}\left\{\frac{r\left(r-\frac{b}{\sin\phi}\right)d^2}{f(r,x+a,d,\phi)}\right\}rdrd\phi\\&+\int_0^{\pi/4}\int_0^{b/\cos\phi}\left\{\frac{r\left(r-\frac{b}{\cos\phi}\right)d^2}{f(r,x-a,d,\phi)}\right\}rdrd\phi+\int_{\pi/4}^{\pi/2}\int_0^{b/\sin\phi}\left\{\frac{r\left(r-\frac{b}{\sin\phi}\right)d^2}{f(r,x-a,d,\phi)}\right\}rdrd\phi\Bigg].\end{aligned} \tag{20}$$

2. The sputtered flux from segment II in Fig. 7

The derivation of the equation for the sputtered flux from segment II in Fig. 7 will be done in the similar way to that of Sec. IV B 1. In this section, only the dark gray triangular region will be discussed in detail, and then the total flux will be derived. First, the limits of the integration of Eq. (12) over r in this area are 0 to $a/\cos\phi$, and those of integration over ϕ are 0 to $\tan^{-1}(b/a)$. Secondly, since the B field is an only function of the y coordinate, the B_r will be

$$B_r=-(\text{const})r\sin\phi(r\sin\phi-b). \tag{21}$$

Hence, the flux from the dark triangular region in Fig. 7 is

$$\Delta H=\int_0^{\tan^{-1}(b/a)}\int_0^{a/\cos\phi}\chi\frac{r\sin\phi(r\sin\phi-b)d^2}{(r^2-2rx\cos\phi+x^2+d^2)^2}\times rdrd\phi. \tag{22}$$

If we use the same notation for the denominator in Eq. (22) with Eq. (20), the total flux from segment II can be expressed as follows:

$$\Delta H_{\rm II}=2\chi\times\left[\int_0^{\tan^{-1}(b/a)}\int_0^{a/\cos\phi}\frac{r\sin\phi\times(r\sin\phi-b)\times d^2}{f(r,x,d,\phi)}rdrd\phi\right.$$
$$+\int_{\tan^{-1}(b/a)}^{\pi/2}\int_0^{b/\sin\phi}\frac{r\sin\phi\times(r\sin\phi-b)\times d^2}{f(r,x,d,\phi)}rdrd\phi+\int_0^{\tan^{-1}(b/a)}\int_0^{a/\cos\phi}\frac{r\sin\phi\times(r\sin\phi-b)\times d^2}{f(r,-x,d,\phi)}rdrd\phi$$
$$\left.+\int_{\tan^{-1}(b/a)}^{\pi/2}\int_0^{b/\sin\phi}\frac{r\sin\phi\times(r\sin\phi-b)\times d^2}{f(r,-x,d,\phi)}rdrd\phi\right]. \quad (23)$$

3. Total flux from rectangular magnetron sputtering

From the discussion in the Secs. IV B 1 and IV B 2, we can obtain an expression for the total flux from the rectangular magnetron shown in Fig. 7. Since it is found to be difficult to solve the equation analytically, some computer works with finite elemental method would be necessary. However, the equation only contains algebraic terms inside itself, so it would not take much time to do such a work.

V. CONCLUSIONS

A simple film thickness uniformity model, which takes the role of magnetic field into account, has been presented. The good agreement between simulated profile and an experimentally measured one was observed. It has been demonstrated that the model has a wide range of applicability to magnetron sputtering systems utilizing a low-pressure gas during the deposition. It may also be found that this simulation can predict the film thickness profile of a magnetron sputtering system with various shapes of magnets before manufacturing of the system with relative ease.

ACKNOWLEDGMENTS

This work was sponsored by a grant from Samsung Electronics, Co., Ltd. The authors appreciate the cooperation of Jang Byungtak, a Ph.D course student of KAIST, with the thickness measurement.

[1] T. Heberlein, G. Krautheim, and W. Wuttke, Vacuum **42**, 47 (1991).
[2] A. A. Fursenko, A. O. Galjukov, Yu. N. Makarov, D. S. Lutovinov, and M. S. Ramm, J. Cryst. Growth **148**, 155 (1995).
[3] Q. Fan, X. Chen, and Y. Zhang, Vacuum **46**, 229 (1995).
[4] S. Swann, Vacuum **38**, 791 (1988).
[5] M. Knudsen, Ann. Phys. (Leipzig) **28**, 999 (1909).
[6] R. J. Gnaedinger, Jr., J. Vac. Sci. Technol. **6**, 355 (1969).
[7] B. Chapman, *Glow Discharge Processes* (Wiley, New York, 1980), pp. 260–270.
[8] S. M. Rossnagel, *Handbook of Plasma Processing Technology*, edited by S. M. Rossnagel, J. J. Cuomo, and W. D. Westwood (Noyes, Park Ridge, 1990), pp. 166–169.
[9] I. S. Gredshteyn and I. M. Ryzhik, *Table of Integrals, Series and Products* (Academic, New York, 1980), pp. 80–83.
[10] S. Dushman and J. M. Lafferty, *Scientific Foundations of Vacuum Technique* (Wiley, New York, 1962), pp. 80–81.
[11] M. A. Liberman and A. J. Lichtenberg, *Principles of Plasma Discharges and Materials Processing* (Wiley, New York, 1994), pp. 47.
[12] M. W. Thompson, Philos. Mag. **18**, 377 (1968).
[13] J. A. Thornton, Thin Solid Films **119**, 87 (1984).
[14] R. S. Robinson, J. Vac. Sci. Technol. **16**, 185 (1979).
[15] S. M. Rossnagel, J. Vac. Sci. Technol. A **6**, 19 (1988).
[16] B. Chapman, in Ref. 7, p. 377.
[17] S. Kadlec and J. Musil, J. Vac. Sci. Technol. A **13**, 389 (1995).